

Probing the Epoch of Reionization with Milky Way Satellites

Joseph A. Muñoz^{1*}, Piero Madau², Abraham Loeb¹, and Jürg Diemand^{2,3}

¹*Harvard-Smithsonian Center for Astrophysics, 60 Garden St., MS 10, Cambridge, MA 02138, USA*

²*Department of Astronomy & Astrophysics, University of California Santa Cruz, 1156 High Street, Santa Cruz, CA 95064, USA*

³*Hubble Fellow*

10 September 2009

ABSTRACT

While the connection between high-redshift star formation and the local universe has recently been used to understand the observed population of faint dwarf galaxies in the Milky Way (MW) halo, we explore how well these nearby objects can probe the epoch of first light. We construct a detailed, physically motivated model for the MW satellites based on the state-of-the-art *Via Lactea II* dark-matter simulations. Our model incorporates molecular hydrogen (H_2) cooling in low-mass systems and inhomogeneous photo-heating feedback during the internal reionization of our own galaxy. We find that the existence of MW satellites fainter than $M_V \approx -5$ is strong evidence for H_2 cooling in low-mass halos, while satellites with $-5 > M_V > -9$ were affected by hydrogen cooling and photoheating feedback. The age of stars in very low-luminosity systems and the minimum luminosity of these satellites are key predictions of our model. Most of the stars populating the brightest MW satellites could have formed after the epoch of reionization. Our models also predict a significantly larger dispersion in M_{300} values than observed and a number of luminous satellites with M_{300} as low as $10^6 M_\odot$.

Key words: Cosmology: theory – early universe – Galaxies: dwarfs

1 INTRODUCTION

According to the standard cold dark matter (CDM) paradigm of cosmic structure formation, massive objects such as the halo of our own Milky Way (MW) grow hierarchically with smaller subunits collapsing earlier and merging to form larger and larger systems over time. Computer simulations have long shown that this merging is incomplete and that the dense cores of such progenitors may survive today as gravitationally bound “subhalos” within their hosts (e.g. Moore et al. 1999). Recently, state-of-the-art simulations have revealed that present-day galaxy halos are extremely lumpy, filled with tens of thousands of surviving substructures on all resolved mass scales (Diemand et al. 2007, 2008; Springel et al. 2008).

The predicted subhalo counts vastly exceed the number of known dwarf satellites of the MW, creating a “missing satellite problem” whose solution within the Λ CDM framework may lie both in the luminosity bias that affects the observed satellite luminosity function (Koposov et al. 2008; Tollerud et al. 2008) as well as in the reduced star form-

ing efficiency predicted for small-mass, dwarf-sized substructure. It is widely accepted that cosmic reionization may offer a plausible mechanism for effectively inhibiting star formation in halos that are not sufficiently massive to accrete warm intergalactic gas, and a number of studies have attempted to interpret the observed population of MW satellites using the process of early, external UV background feedback (Bullock et al. 2000; Benson et al. 2002; Somerville 2002; Kravtsov et al. 2004; Moore et al. 2006; Strigari et al. 2007; Simon & Geha 2007; Madau et al. 2008a; Busha et al. 2009; Macciò et al. 2009a).

Lately, it has been suggested that a detailed quantitative resolution of the “missing satellite problem” may require some “pre-reionization” suppression mechanism to avoid producing too many faint Galactic dwarf spheroidals (dSphs). Using results from the *Via Lactea II* (VLII) simulation, Madau et al. (2008b) showed that thousands of surviving subhalos in the halo of the MW today have progenitors massive enough for their gas to cool via excitation of H_2 and fragment *prior to the reionization epoch*, which they assumed occurred around $z \sim 10$. In addition, they found that star formation in these objects must have been extremely inefficient converting only a small fraction of

* E-mail: jamunoz@cfa.harvard.edu

their gas into stars or having a top-heavy initial mass function (e.g. Abel et al. 2002). Similar conclusions have been reached by Koposov et al. (2009).

Inspired by these results, we develop a detailed, astrophysically motivated model for the formation of dSphs. We consider a general scenario in which H_2 fragmentation can shut off before the suppression of atomic hydrogen cooling during reionization and include post-reionization star formation in the largest subhalos. This work is unique in that it considers the possibility that the MW was self-reionized from the inside out, which further suppresses the amount of stars produced in progenitors with $M > 10^8 M_\odot$. This assumption is in agreement with observations that the mean-free-path of ionizing radiation through intervening Lyman-limit systems (LLSs) is much less, at $z > 7$, than the 20Mpc distance between the Virgo Cluster and the MW (Faucher-Giguère et al. 2008). Using this physical model with the most recent observations of the ultra-faint MW satellites found in the *Sloan Digital Sky Survey* Data Release 5 (SDSS DR5) as a probe of both reionization and early star formation physics, differentiates our work from previous studies that focused on the properties of dSphs. In this work we adopt subhalo catalogs from the one billion particle VLII simulation, which allow us to track the progenitors of surviving present-day MW substructure far up in the merger hierarchy than done before. The unprecedented mass resolution, combined with the fossil signatures of the reionization epoch in the Galactic halo, allows us to study gas cooling in the early universe, star formation in the first generation of galaxies, and the baryonic building blocks of today's galaxies.

This *Paper* is organized as follows. In §2, we briefly describe the VLII simulation and develop our model. In §3, we compare the results with observations, examine which observables best constrain model components, and determine model parameters. Finally, we summarize our conclusions and discuss how they contribute to our understanding of reionization and high-redshift star formation in §4.

2 BASIC MODEL

The recently completed VLII simulation (Diemand et al. 2008) uses just over a billion dissipationless particles each weighting $4,100 M_\odot$ to simulate the formation of a $M_{200} = 1.9 \times 10^{12} M_\odot$ MW-sized halo in a *Wilkinson Microwave Anisotropy Probe* (WMAP) 3-year cosmology (Spergel et al. 2007). It resolves 50,000 subhalos today within the host's $r_{200} = 402$ kpc (the radius enclosing an average density 200 times the mean matter value) and tracks the merger history of each subhalo that survives to the present epoch through 400 time slices between $z = 27.54$ and today. In this study, we analyze catalogs that, for each surviving subhalo, give the number of progenitors and their masses at a given redshift. The details of the progenitor determinations are given in Madau et al. (2008b). Progenitors are resolved down to masses of $10^5 M_\odot$, almost a factor of 200 better than the dissipationless simulation of the MW used by Gnedin & Kravtsov (2006). This extra resolution allows us to incorporate physical models involving H_2 cooling in very low-mass halos at extremely high redshift.

Our model for assigning stars and luminosities to MW

subhalos from the VLII catalogs involves carefully charting the state of cosmic hydrogen and a comparison of the cooling mass with the Jeans mass throughout cosmic time. We identify four epochs of star formation that can contribute to the stellar populations of MW dSphs: (1) stars can form at $z \sim 20$, well before reionization, in systems large enough for the cooling of molecular hydrogen; (2) H I cooling produces stars before reionization that are responsible for photoheating the IGM; (3) further cooling via H I from reionization to $z \sim 2$ produces stars in subhalos large enough to hold onto their gas; and (4) stars form in the last 10 Gyr from metal cooling. In the following subsections, we describe the process of star formation in each of the above epochs following Barkana & Loeb (2001), and detail how we attach stellar populations to the simulation subhalos. In incorporating this model, we use the set of best-fit cosmological parameters from the WMAP 5-year data release (Komatsu 2009), which are fully consistent with the previous results from WMAP3.

2.1 Epoch of Molecular Hydrogen Cooling

In the pristine early universe beyond $z \sim 20$, cooling via H_2 is efficient in systems with total halo masses as low as $M_{H_2} \sim 5 \times 10^4 M_\odot$, while the Jeans mass is lower by an order of magnitude (Barkana & Loeb 2001). The resulting first stars create a background of Lyman-Werner photons, which both dissociates H_2 and acts as positive feedback to replenish it (Ricotti et al. 2002a,b). Supernova explosions from these stars also begins to enrich the IGM with the small amount of heavy metals necessary for metal cooling.

Ultra-faint MW dwarf satellites are a natural and unavoidable consequence of H_2 cooling in the pre-reionization universe (Ricotti & Gnedin 2005; Bovill & Ricotti 2008), and this mechanism can be responsible for the low observed metallicities of these objects (Salvadori & Ferrara 2008). We take advantage of the high mass resolution of VLII to trace the pre-reionization progenitors of these ultra-faint dwarfs, for the first time, down to an H_2 cooling mass as small as $10^5 M_\odot$ to make quantitative predictions about their abundance and observable properties.

Motivated by Madau et al. (2008b), where an extremely small star formation efficiency was invoked in $< 10^7 M_\odot$ objects at $z = 11$ to avoid overpopulating the faint end of the MW satellite luminosity function (LF), we allow for the possibility that H_2 cooling is suppressed earlier than H I cooling (Haiman et al. 1997, 2000). Earlier suppression could explain the very small efficiency of these small objects in a very natural way since the halos able to cool via molecular hydrogen would be less numerous at early times. Whalen et al. (2008) have suggested that this suppression may occur around $z \sim 20$ and result from supernova feedback.

We assume a redshift, z_{H_2} , after which H_2 cooling is quenched, and a mass threshold for halos, M_{H_2} , below which such cooling is inefficient. We consider the VLII redshift snapshots at $z = 17.9$ and $z = 23.1$ as possible values for z_{H_2} and extract from the halo catalogs all surviving MW subhalos at $z = 0$ with progenitors above M_{H_2} at z_{H_2} . We further assume that a fraction $f_b = \Omega_b/\Omega_M \approx 0.16$ of the total mass in each progenitor is in gas. Due to the metal-poor state of the primordial gas, the first generation

of Population III stars has a top-heavy initial mass function (IMF) and does not survive to the present day. Rather, the deaths of these stars seed the gas with traces of metals and spawn a new, metal-cooled stellar population with a Salpeter IMF. While these metal-cooled stars are the ones with local relics seen today, the system initially must have satisfied the conditions for H_2 cooling. We assume that, through this process, a fraction f_{H_2} of the initial gas is converted into stars with a Salpeter IMF; this factor accounts for any gas that may have been expelled by supernovae. The low-mass stellar population will survive to the present day with a visual luminosity of $M_V = 6.7^1$ per solar mass of initial stars (Bruzual & Charlot 2003; Madau et al. 2008b). For each surviving subhalo, we sum up the stars contributed by each progenitor at z_{H_2} . We assume that these stars are quickly incorporated into the center of the forming subhalo so that they are not stripped during subsequent mergers or tidal encounters with the MW.

2.2 Atomic Hydrogen Cooling Before Reionization

Next, we discuss the formation of stars in subhalos from H I cooling prior to the photoheating of the IGM at reionization. This cooling process is very efficient only in gas with temperatures above $T_4 \equiv 10^4 \text{ K}$. Before the IGM photoheats to approximately T_4 , this temperature requirement limits H I cooling to halos whose virial temperatures exceed T_4 or, equivalently, to those with halo masses above $M_4 = 10^8 M_\odot [(1+z)/10]^{-3/2}$ (Barkana & Loeb 2001). Stars formed in this way are responsible for producing the N_{clump} photons required on average to reionize each atom of H I in the Universe. This happens when the collapse fraction of halos with $M > M_4$ exceeds a critical threshold (Barkana & Loeb 2004). Thus, the condition for the average reionization redshift of the universe, \bar{z}_{rei} , is:

$$N_{\text{clump}} \Omega_b \rho_{\text{crit}} = N_\gamma f_{\text{H I}} f_b \int_{M_4}^{\infty} dM' M' \frac{dn}{dM'}(M', \bar{z}_{\text{rei}}), \quad (1)$$

where dn/dM is the comoving mass function of halos, N_γ is the number of ionizing photons produced per baryon in stars, $f_{\text{H I}}$ is the fraction of gas turned into stars by H I cooling, and ρ_{crit} is the critical density of the universe today. Here, $\Omega_b \rho_{\text{crit}}$ represents the total comoving mass density of baryons in the Universe to be reionized, not just those in underdense or mean-density regions. Therefore, the standard factor f_{esc} , the fraction of ionizing photons that escape into the IGM, does not appear on the right-hand side of equation 1. Using the Sheth & Tormen (1999) mass function for halos, we can solve for the combination $Q \equiv N_\gamma f_{\text{H I}}/N_{\text{clump}}$

¹ We set a minimum stellar mass of $0.1 M_\odot$ for the Salpeter IMF. However, in principle, the cosmic microwave background creates a temperature floor to any cooling process that may in turn determine the minimum mass of stars at high redshifts (Bromm & Loeb 2003; Bromm & Larson 2004). In our discussion, we implicitly assume that stars at this lower limit would survive to the present day (or equivalently that this limit is below $\sim 1 M_\odot$). In this regime, the luminosity per unit mass is not very sensitive to the value of the low-mass cutoff of the Salpeter mass function.

given any value of \bar{z}_{rei} . For $\bar{z}_{\text{rei}} = 11$, approximately the best fit WMAP5 value of the mean reionization redshift, we find $Q \sim 100$.

After reionization, the IGM is rapidly photoheated to $\sim 10^4 \text{ K}$. Halos with masses less than the filtering mass, M_F , can no longer hold onto their gas or accrete new baryonic material (Gnedin 2000). While Kopesov et al. (2009) adopted the expression of Gnedin (2000) for the remaining gas available for star formation, Busha et al. (2009) correctly pointed out that only cold gas can actually form stars. The situation is made worse by infalling gas whose temperature increases by an extra order of magnitude during collapse. Thus, after reionization, only gaseous halos with virial temperatures above $T_5 = 10^5 \text{ K}$ may cool via H I to form additional stars (see §2.3).

As in §2.1, we compile a list of surviving MW subhalos at $z = 0$ and all of their progenitors with $M > M_4$ at \bar{z}_{rei} and assign to each a stellar mass M_\star and a luminosity (today, after more than 13 Gyr of cosmic time) of $M_V = 6.7$ per solar mass of stars distributed with a Salpeter IMF. Our choice of IMF constrains $N_\gamma = 4000$ (Bromm et al. 2001). As before, we assume that partial tidal stripping of their hosts at later times does not remove these deeply embedded stars. Present-day subhalos with $M > M_4$ progenitors at \bar{z}_{rei} as well as earlier progenitors at z_{H_2} with $M > M_{\text{H}_2}$, as outlined in §2.1, have contributions to their stellar populations from both epochs.

We now consider two alternatives for the reionization history of the MW galaxy-forming region (MWgfr) that affect the calculation of M_\star . Alvarez et al. (2009) suggest that the MW was most likely ionized externally by radiation from the Virgo Cluster. However, they do not include the effect of intervening LLs, which absorb external UV photons and may allow the MWgfr to reionize from the inside out instead. Here we consider and present results for both scenarios.

If the MWgfr was reionized externally by the Virgo Cluster, we would expect the ionization front to cross the region very quickly. In this case, we can assume that the region reionized promptly at \bar{z}_{rei} , and consider the subhalo progenitors at that redshift. The mass in stars formed by each subhalo progenitor at \bar{z}_{rei} is the same as that assumed by Madau et al. (2008b),

$$M_\star = f_{\text{H I, ex}} f_b M_{\text{halo}}, \quad (2)$$

where the subscript “ex” denotes the assumption of external reionization. Considering only stars that formed through the H I cooling of gas before $z = 11$ and assuming a Salpeter IMF, Madau et al. (2008b) found that a star formation efficiency of $f_{\text{H I}} \approx 0.02$ for progenitors with $M_{\text{halo}} > 7 \times 10^7 M_\odot$ would reproduce the observed satellite LF.

On the other hand, if the MWgfr was ionized internally, different parts of it would have reached the critical collapse fraction of H I -cooling halos necessary for reionization at different times due to their respective overdensities (Barkana & Loeb 2004). Thus, there should be fluctuations in the redshift of reionization within the MW itself about the mean at \bar{z}_{rei} , an effect that has not been considered in the literature. Each subhalo progenitor will photoionize and reheat its own gas content at the time when it has produced N_{clump} ionizing photons per hydrogen atom. This condition

is met when

$$M_{\star} = \frac{N_{\text{clump}} g(\delta)}{N_{\gamma} (1 - f_{\text{esc}})} f_b M_{\text{halo}} = \frac{f_{\text{HI}} g(\delta)}{Q (1 - f_{\text{esc}})} f_b M_{\text{halo}}, \quad (3)$$

where $g(\delta)$ gives the ratio of N_{clump} in the overdense progenitor to the average N_{clump} in the universe. The factor $(1 - f_{\text{esc}})$ selects only those photons that do not escape from the overdense progenitor and can be used to photoionize it. Equation 3 tells us how much stellar mass to assign a progenitor of mass M_{halo} . Each progenitor, A, has its own $M > M_4$ progenitors, B, that form stars at redshift $z'_{\text{rei}} > \bar{z}_{\text{rei}}$, before system A collapses at \bar{z}_{rei} . Baryonic material from the region that formed the A progenitor not converted into stars at z'_{rei} is photoionized before it can be incorporated into A at \bar{z}_{rei} and cannot form stars unless progenitor A eventually reaches a mass of M_5 , the mass corresponding to a virial temperature of T_5 or a circular velocity of $V_5 = 52 \text{ km s}^{-1}$. However, we expect most of the gas in B progenitors with $M > M_4$ at z'_{rei} to form stars.

Accounting for the inside-out morphology of the MWgfr reionization provides a natural explanation for the low values of $f_{\text{HI,ex}}$ found by several studies (Madau et al. 2008b; Koposov et al. 2009; Busha et al. 2009), which assumed a single value for the reionization redshift of the entire MWgfr. Since stellar mass is a linear function of halo mass in both equations 2 and 3, both morphologies fit the same observed LF when

$$f_{\text{HI,ex}} = \frac{f_{\text{HI}} g(\delta)}{Q (1 - f_{\text{esc}})}. \quad (4)$$

If $f_{\text{HI}} g(\delta)/(1 - f_{\text{esc}})$ is of order unity at $\bar{z}_{\text{rei}} = 11$, we find that $f_{\text{HI,ex}} \approx 0.01$. We can understand this physically by considering how, at the redshift of star formation suppression, a lower efficiency is equivalent to a smaller amount of matter in collapsed objects (smaller M_{halo} in Eq. 2) in terms of calculating how much stellar mass is produced. We see from this that, for a given average redshift of reionization in the MWgfr, the inside-out and outside-in morphologies fit the luminosity function equally well but result in different interpretations of the fitting parameters.

2.3 Star Formation After Reionization

We assume that cosmic reionization and the photoheating of the MWgfr completes rapidly after \bar{z}_{rei} . Subsequently, only halos that have accumulated a mass of $M_5 > 1$ are able to hold onto their gas long enough for it to form further stars via HI-cooling. We assume that this star formation is quenched when the subhalo begins to interact with the MW host. The merger histories of each surviving MW subhalo at $z = 0$ show only eight subhalos that achieved a maximum circular velocity greater than V_5 at some point in their histories. We determine the redshift at which the maximum circular velocity reaches its peak. The subsequent reduction is due to tidal interactions during infall into the MW host with both neighboring dwarfs and the host itself (Kravtsov et al. 2004) that we assume coincide with the quenching of star formation through ram pressure. In agreement with Koposov et al. (2009), we find that this mass loss typically occurs around $z = 2 - 4$ (in five of our eight subhalos) but can happen as early as $z = 8$ and as late as $z = 1.6$.

We add an additional mass of $f_5 f_b M_{\text{max}}$ worth of stars

minus the mass of any stars formed in either of the first two epochs to each subhalo whose peak circular velocity exceeds V_5 . Here, f_5 is an efficiency parameter for star formation during this epoch that takes into account how much of the hot gas is cooled to form stars and how much of the gas mass is removed during infall. M_{max} is the virial mass corresponding to the maximum value of the circular velocity for each subhalo. We calculate the age of these new stars from the redshift at which the subhalo attains its maximum circular velocity and use this age to calculate the luminosity of each solar mass of stars from Bruzual & Charlot (2003).

2.4 Recent Star Formation

The final episode of star formation that we include in our model occurs in the last 10 Gyr since $z = 1.6$. Since we are interested primarily in the physics of the early universe, we do not attempt to develop here a detailed model for the production of these stars but presume that metal cooling is involved and use the observations of Orban et al. (2008) to add additional young stars in a stochastic way.

For each of the classical, pre-SDSS MW satellite, Orban et al. (2008) have measured f_{10G} , the fraction of stellar mass produced in the last 10 Gyr, and τ , the mass-averaged stellar age. They find that the metallicities of the ultra-faint, SDSS satellites are so low that no star formation is expected for these in the last 10 Gyr. As we will show, subhalos that achieve a maximum circular velocity of at least V_5 are associated only with the classical MW satellites studied by Orban et al. (2008), while stars that formed prior to reionization populate both the classical and SDSS dSphs. Therefore, we set $f_{10G} = 0$ for subhalo progenitors that only formed stars before reionization to be consistent with these metallicity observations. However, setting this constraint only for progenitors with H_2 -induced cooling does not significantly change our results.

The cumulative probability distribution of f_{10G} is approximately linear with a linear fit reaching unity at $f_{10G} = 0.89$ (Orban et al. 2008). Thus, for each subhalo with stars that formed after reionization, as outlined above, we select a value for f_{10G} at random from a flat probability distribution within the interval $[0.00, 0.89]$. The mass of stars produced since $z = 1.6$ is, therefore, given by $f_{10G}/(1 - f_{10G})$ times the mass of stars produced from the mechanisms outlined in the previous three subsections.

If we pretend that all of the stars formed in the MW satellites prior to $z = 1.6$ have an age of 14 Gyr, we can use the measured values of f_{10G} and τ to estimate the mass-weighted average age of those stars formed in the last 10 Gyr. We find that the stars that formed after $z = 1.6$ in each satellite have ages between 1 Gyr and 8 Gyr with an average around 5 Gyr. Since the luminosity per solar mass of a stellar population does not vary much in this age range (Bruzual & Charlot 2003), we assume a fixed age of 5 Gyr for the recent stars formed in each of our subhalos. Bruzual & Charlot (2003) give the luminosity of a stellar population with this age as $M_V = 5.8$ per solar mass.

3 COMPARISON WITH OBSERVATIONS

We are now at a position to compare the properties of the luminous subhalos in our model with observations of MW dwarf satellites. These include values for Segue II, the newest MW satellite discovered in the SDSS data (Belokurov 2009), but exclude Leo T which, at a distance of 417 kpc from the Sun, is outside the viral radius of the VLII simulation. The simulation abundance calculations represent mean values about which there is Poisson scatter. However, for clarity in the plots, we instead assign Poisson errors on the observational data as if the observed count were the mean value. We ignore the variations that would be expected in different cosmological realizations of the MW and leave this analysis to future work.

In §3.1, we first outline the observational biases of our observed sample of satellites and describe how we apply a similar bias to the simulated population to account for the completeness of the sample. We then proceed to compare the simulated and observed LF of satellites in §3.2, and investigate how this important observable constrains our model. Finally, we consider how well our model reproduces other observables in §3.3 such as the radial distribution of satellites within the MW halo, the mass of a satellite within 300 pc of its center, and a satellite’s mass-to-light ratio.

3.1 Observational Completeness

Our sample includes two sets of MW satellites: those discovered prior to SDSS and the ultra-faint sample found in the SDSS DR5. However, the observational biases for the two samples are not the same. Not only is the SDSS sample complete only to a given surface brightness threshold, but the SDSS footprint only covers 20% of the sky. Rather than apply corrections to the observed distribution functions of satellites to account for the total population as in Tollerud et al. (2008), we follow Madau et al. (2008b) in adjusting our simulated population to represent those objects that would be detected by SDSS.

The observational completeness of the SDSS DR5 was modeled by Koposov et al. (2008) and Tollerud et al. (2008) by defining the maximum radius at which a satellite of a given visual magnitude would be observed. This radial threshold is given by:

$$r_{\max} = \left(\frac{3}{4\pi f_{\text{DR5}}} \right)^{1/3} 10^{(-0.6 M_V - 5.23)/3} \text{ Mpc}, \quad (5)$$

where $f_{\text{DR5}} = 0.194$ is the fraction of the sky covered by DR5. We exclude each subhalo in our simulation with a distance beyond this threshold for its particular luminosity. Moreover, when plotting the luminosity and radial distribution functions of satellites in §3.2 and §3.3, we correct these distribution by an additional factor of f_{DR5} . The observed distributions are also corrected so that each classical MW satellite contributes only f_{DR5} to the total abundance, while each SDSS satellite contributes fully. However, all observed satellites contribute equally when calculating the fractional Poisson errors in the distribution functions.

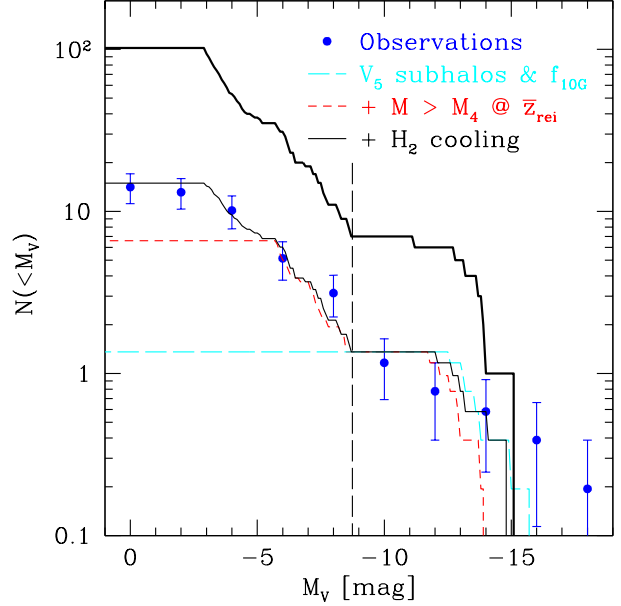


Figure 1. The luminosity function (LF) of MW satellites. Thin lines show abundances in the SDSS footprint with the DR5 selection threshold. The observed function is shown by the blue points with the non-SDSS objects each contributing a fractional amount $f_{\text{DR5}} = 0.194$ to the total. The curves show the theoretical predictions including successively more elaborate models. The model given by the long-dashed, cyan curve illuminates only those VLII subhalos with maximum circular velocities that exceed V_5 at some point in their histories and continue to form stars after reionization via atomic hydrogen cooling (with an efficiency of $f_5 = 0.02$) and metal cooling in the last 10 Gyr ($f_{10G} \neq 0$). The short-dashed, red curve includes star formation in subhalo progenitors more massive than M_4 at $z_{\text{rei}} = 11.2$ assuming a single redshift of reionization for the entire MWgfr and $f_{\text{H,ex}} = 0.02$. The thin solid, black curve fitting the faint end of the observed LF additionally takes into account molecular hydrogen cooling, prior to suppression at $z_{\text{H}_2} = 23.1$, in progenitors more massive than $M_{\text{H}_2} = 10^5 M_\odot$ with $f_{\text{H}_2} = 0.4$. The thick, solid, black curve represents the same model as the thin, solid one, but now all satellites in the MW halo out to the virial radius are shown, not just those that meet the SDSS criteria. The long-dashed vertical line demarcates the luminosities at which pre- vs. post-SDSS satellites are observed.

3.2 The Luminosity Function

First, we would like to compare our simulated LF of MW satellites to the observed distribution and explore the importance of this observable for constraining model parameters.

The observed and simulated LFs are shown in Figure 1. We present multiple theoretical curves, each of which includes additional layers of the model to demonstrate the relationship between the model and the predictions. For example, taking into account only subhalos that reach a maximum circular velocity of at least V_5 at some point in their histories (see §2.3 and §2.4) with $f_5 = 0.02$ roughly reproduces the LF of pre-SDSS satellites. Recent, high-metallicity star formation in the last 10 Gyr introduces some stochasticity in the theoretical LF, but the fluctuations are smaller than the observed errors. However, this limited model fails to account for observed satellites dimmer than $M_V \approx -9$.

The addition of star formation in progenitors with $M > M_4$ before reionization at $\bar{z}_{\text{rei}} = 11.2$ extends the agreement between the theoretical and observed LFs down to $M_V \approx -6$ when we assume $f_{\text{H I, ex}} = 0.02$ in an external reionization model or $N_{\text{clump}} g(\delta) (1 - f_{\text{esc}}) \approx 30$ in an inside-out model. Additionally, the inclusion of pre-reionization stars lowers the post-reionization efficiency to $f_5 = 0.01$.

However, it is only with the inclusion of stars in low-mass molecular hydrogen cooling systems that the model output reproduces observations of ultra-faint satellites. This element of our model and its ability to explain and be constrained by the data is a major new development in this work that distinguishes it from other studies in the literature. In Figure 1, we assumed $z_{\text{H}_2} = 23.1$ and $M_{\text{H}_2} = 10^5 M_\odot$ with $f_{\text{H}_2} = 0.4$. The model not only gives the correct abundance of satellites brighter than the faintest known object, Segue 1, it also provides an explanation for why no fainter objects have been found. To produce stars, our model requires a subhalo to have at least one progenitor with mass above the cooling mass for molecular hydrogen. The fewest stars are produced when the subhalo has exactly one of these progenitors that is just above M_{H_2} . In this case, the mass in stars is $M_* = f_{\text{H}_2} f_b M_{\text{H}_2} \approx 6600 M_\odot$, and the luminosity today is $M_V > -2.8$. The existence of a satellite as dim as Segue 1 is within the uncertainty of our approximations. While a precise measurement of the lower limit on the luminosity of MW satellites in the future will provide a tighter constraint on early star formation, our model implies that the exact value cannot be significantly below what has already been observed.

We emphasize this intriguing result that star formation from different time periods, before the suppression of H_2 cooling and before and after reionization, are required to fit the theoretical LF to the data at the faint, middle, and bright ends, respectively. Although some objects do have stars from multiple epochs, they are typically dominated by the processes in a single part of the model. This helps prevent degeneracy among all of our different parameters and allows us to learn about star formation parameters in each stage almost independently of the others.

So far, we have produced results by fixing $z_{\text{H}_2} = 23.1$ and $\bar{z}_{\text{rei}} = 11.2$ and varying the efficiencies and mass thresholds to obtain agreement. However, by allowing for different values of the suppression redshifts, we can arrive at new sets of parameters that allow the model to fit the observed LF.

Figure 2 compares the simulated LFs with reionization fixed at three consecutive VLII slices for which progenitor analysis is available: $\bar{z}_{\text{rei}} = 7.77$, 9.14, and 11.2. For each of these redshifts, we find $Q = 28$, 46, and 130. We have fixed $z_{\text{H}_2} = 23.1$ and $M_{\text{H}_2} = 10^5 M_\odot$ but varied $N_{\text{clump}} = N_\gamma f_{\text{H I}}/Q$ and f_{H_2} to find the values resulting in the closest fit to the data. For convenience we define $N'_{\text{clump}} \equiv N_{\text{clump}} g(\delta)/(1 - f_{\text{esc}})$ and $f'_{\text{H I}} \equiv f_{\text{H I}} g(\delta)/(1 - f_{\text{esc}})$. Our sets of fit parameters, then, are $(\bar{z}_{\text{rei}}, N'_{\text{clump}}, f'_{\text{H I}}, f_{\text{H}_2}) = \{(7.77, 7, 0.05, < 0.001), (9.14, 17, 0.2, 0.1), (11.2, 30, 1, 0.4)\}$; the values of $f_{\text{H I, ex}}$ for an external reionization scenario can be calculated from equation 4.

At earlier times, less mass in the Universe is in collapsed objects above the cooling mass. This results in a monotonically increasing value of Q with \bar{z}_{rei} since each baryon in these objects must ionize a larger number of hydrogen

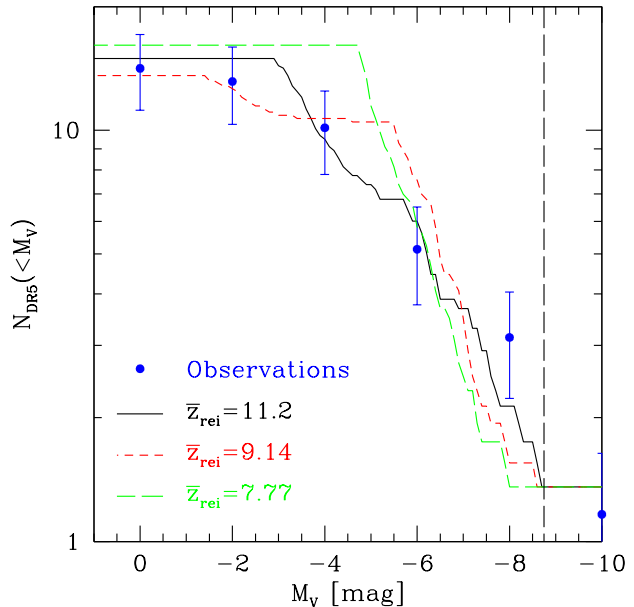


Figure 2. The faint end of the luminosity function of MW satellites in the SDSS footprint with the DR5 selection threshold. The observed function is shown by the blue points with the non-SDSS objects each contributing a fractional amount $f_{\text{DR5}} = 0.194$ to the total. The curves show the theoretical predictions for different values of \bar{z}_{rei} with $z_{\text{H}_2} = 23.1$ and other model parameters optimized to produce the best agreement with luminosity function data. The solid, black; short-dashed, red; and long-dashed, green curves have $\bar{z}_{\text{rei}} = 11.2$, 9.14, and 7.77, respectively. The long-dashed vertical line demarcates the luminosities at which pre- vs. post-SDSS satellites are observed.

atoms. This requires the universe to be *less* clumpy for fixed $f_{\text{H I}}$. However, the reduction in the mass contained in each present-day subhalo’s progenitors as \bar{z}_{rei} increases requires larger values of $f'_{\text{H I}}$ to produce the same observed stellar mass today. This effect produces global reionization more efficiently and allows *increased* clumping. Since $f'_{\text{H I}}$ increases faster with \bar{z}_{rei} than does Q , the net result is an increasing N'_{clump} .

Because later reionization allows for star formation in more objects near the cooling threshold before H I cooling is suppressed, star formation in molecular hydrogen cooling halos at earlier redshifts is allowed to be less efficient to produce roughly similar LFs. This is responsible for the reduced values of f_{H_2} that we find for lower \bar{z}_{rei} . The value $f_{\text{H}_2} < 0.001$ effectively means that the contribution of stars in molecular hydrogen cooling systems before z_{H_2} to the luminosity of MW satellites is negligible; this results in an absence of satellites with luminosities fainter than $M_V \approx -5$.

While all three considered values of \bar{z}_{rei} produced similar totals for the number of observed MW satellites, the LF slope between $-5 > M_V > -9$ seems to favor earlier reionization around $\bar{z}_{\text{rei}} = 11$.

We also considered the effect of varying z_{H_2} and examined two VLII slices at $z = 17.9$ and 23.1. We fixed the reionization parameters to be those best fit for $\bar{z}_{\text{rei}} = 11.2$, but varied M_{H_2} and f_{H_2} to find the best agreement with the LF data. Figure 3 shows the resulting LFs and compares them with observations. The model with parameters

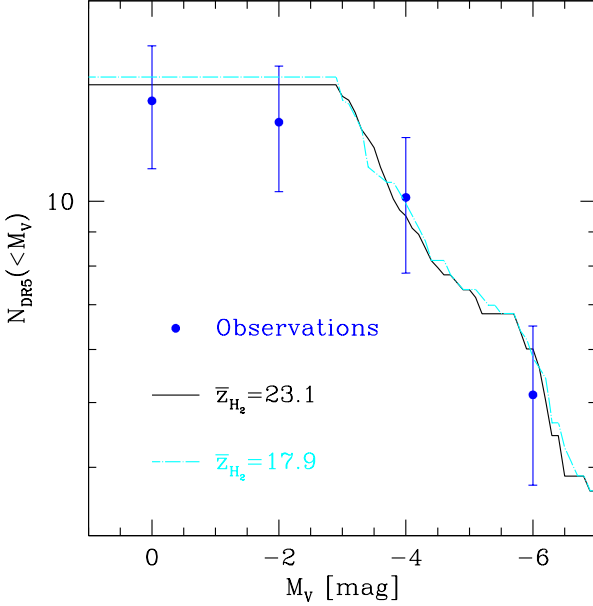


Figure 3. Same as Figure 2 except we have fixed $\bar{z}_{\text{rei}} = 11.2$ and the solid, black and dot-dashed cyan curves show theoretical predictions for sets of parameters given $z_{\text{H}_2} = 23.1$ and 17.9 , respectively.

set at $(z_{\text{H}_2}, M_{\text{H}_2}/M_{\odot}, f_{\text{H}_2}) = (23.1, 10^5, 0.4)$ produces almost identical results as that with $(17.9, 10^6, 0.04)$. Allowing more time for stars to form before the suppression of H_2 cooling is compensated for by a larger cooling mass threshold and a smaller star formation efficiency. The minimum cooling masses for the redshifts we considered are around the minimum masses typically assumed in simulations of feedback from the first stars (Whalen et al. 2008).

3.3 Radial Distribution, M_{300} , and M/L

Given the degeneracies of various degrees that we have seen in the LF for some sets of model parameters, we attempt to use the other observables to learn more about the early universe. Figure 4 shows the radial distribution throughout the MW of the observed and simulated satellites for different pairs of fixed $(\bar{z}_{\text{rei}}, z_{\text{H}_2})$ with other model parameters optimized to produce the best agreement with luminosity function data. We find that all of the $z_{\text{H}_2} = 23.1$ models are fairly consistent with the radial data deviating non-negligibly only for satellites in the range $50 < r/\text{kpc} < 100$ of the MW center. The $(\bar{z}_{\text{rei}}, z_{\text{H}_2}) = (11.2, 17.9)$ prediction for the radial distribution rises more sharply than expected for $r < 100$ kpc, but the statistical strength of this deviation is by no means overwhelming.

We further explored whether these parameter sets were distinguishable in the distribution function of the maximum circular velocity of the subhalos. This property is difficult to measure observationally from the velocity dispersion of real satellites at a given radius from the center of the object. However, no significant difference was found among the distributions for model parameters that also fit the LF data.

In addition to considering distribution functions, we would also like to test for agreement between our model

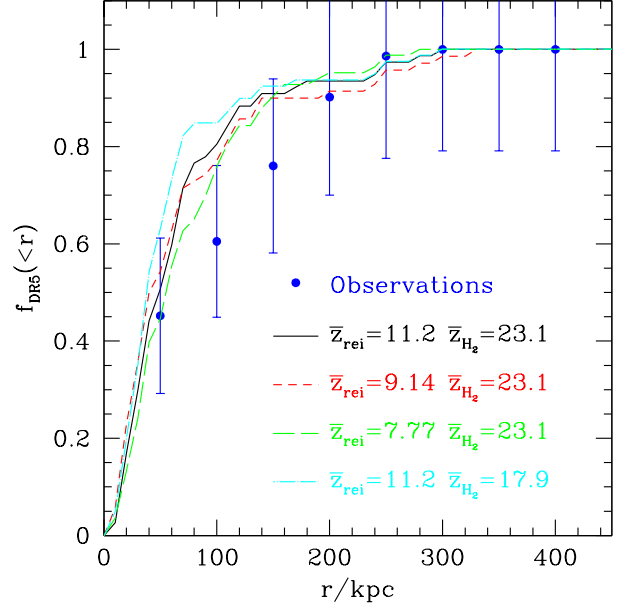


Figure 4. The radial distribution function of MW satellites in the SDSS footprint with the DR5 selection threshold. The profile is plotted as the fraction of the total within a given radius. The observed profile is given by the blue points with the non-SDSS objects each contributing an amount $f_{\text{DR5}} = 0.194$ to the total. The curves show the theoretical predictions for different pairs of fixed $(\bar{z}_{\text{rei}}, z_{\text{H}_2})$ with other model parameters optimized to produce the best agreement with luminosity function data. The solid, black curve has $(11.2, 23.1)$, the short-dashed, red curve $(9.14, 23.1)$, the long-dashed, green curve $(7.77, 23.1)$, and the dot-dashed, cyan curve $(11.2, 17.9)$.

and observations of specific satellite properties. The mass enclosed within 300 pc, M_{300} , as a function of luminosity has been studied using both observational (Mateo 1998; Gilmore et al. 2007; Strigari et al. 2008) and theoretical (Li et al. 2008; Koposov et al. 2009; Macciò et al. 2009b) approaches that hinted at a characteristic mass scale for MW satellites of about $10^7 M_{\odot}$. Both the relatively constant value of M_{300} and the extreme observed mass-to-light ratios of the faintest satellites are properties of the population that we would like our model to reproduce, however, we keep in mind that both M_{300} and the total mass from which mass-to-light ratios are calculated are difficult to determine observationally.

In Figure 5, we present measurements of M_{300} for MW satellites from Strigari et al. (2008) and compare them with the output from our $(\bar{z}_{\text{rei}}, z_{\text{H}_2}) = (11.2, 23.1)$ model. Figure 6 similarly compares the observed mass-to-light ratios for each satellite (Mateo 1998; Simon & Geha 2007; Martin et al. 2007) with the value calculated using the simulated mass within its tidal radius. Both M_{300} and the mass-to-light ratio are plotted as a function of satellite V-band luminosity taken from Tollerud et al. (2008), whose values are a little more up-to-date than those in Strigari et al. (2008). While we continue to apply the SDSS DR5 selection criterion from equation 5, we plot all of the illuminated subhalos across the sky from our model in both figures rather than select only 20% in the SDSS field-of-view. However, we simply omit

known satellites for which we were unable to find reliable estimates of the relevant data.

While our model predicts a fairly constant M_{300} as a function of luminosity (a variation of about an order-of-magnitude over six decades in luminosity), there is still some disagreement at low luminosities where we find a lower average M_{300} and greater scatter than observed. We find that values of M_{300} measured directly from the simulation match very well with those obtained assuming, for each satellite, an NFW profile (Navarro et al. 1997) fit to its simulated maximum circular velocity and the radius at which this maximum is reached. A power-law fit to the resulting scatter plot of M_{300} vs. V-band luminosity, L_V , of the form $M_{300} = \beta L_V^\alpha$ yields $\alpha = 0.22$ for both the simulated and NFW values of M_{300} . This is much steeper than the value of $\alpha = 0.05$ for the Strigari et al. (2008) measured values of M_{300} with the up-to-date values of L_V .

Assuming that the NFW profile is a good fit for all subhalos at all times, we also calculated M_{300} for each subhalo at the redshift when the evolution in its maximum circular velocity reaches its peak. The difference between peak and present values should give us an idea of how much tidal stripping changes the mass estimates. Macciò et al. (2009b) recently suggested that tidal stripping would result in a flattening of the $M_{300} - L_V$ relation. However, our results show a further steepening as more low-luminosity subhalos lose a significant amount of their mass than do high luminosity ones. We find $\alpha = 0.15$ for the early values of M_{300} . While it is true that large, low-concentration systems lose more total mass to tidal stripping than smaller ones do, they are actually denser and more robust to stripping at a fixed radius. Additionally, if the smaller subhalos are also initially fainter, they must be deeper in the inner halo to be detected (i.e. have smaller r_{max}) where tidal effects are stronger, while larger, brighter halos can be detected even at large radii where tides are weak.

Of course, an NFW profile is not always a good fit for all subhalos at all times. For example, if the peak in the maximum circular velocity is reached during a merger, one can get a rather large radius as well, which results in a low concentration and low M_{300} . The actual mass distribution during a merger is quite different from NFW, and the true M_{300} would be higher. This explains why a few of the subhalos plotted in Figure 5 appear to gain mass from the peak until today. However, if we were able to plot the true, larger values of M_{300} at the time of the peak circular velocity for all subhalos, it would only show a greater steepening between the epoch when the peak is reached and today.

The tension at low luminosities between our predictions and the measurements of Strigari et al. (2008) may well be explained by the difficulty in determining M_{300} observationally. The tracer stars in many small systems do not extend past 100 pc and converting the mass within this radius to that inside 300 pc requires assumptions about the dark matter distribution (e.g. shape, orientation, density profile) and about the orbits of the stars. Additionally, interlopers and/or undifferentiated binary stars could systematically skew velocity dispersion measurements, especially in those satellites where the dispersion is small (~ 5 km/s). These errors could significantly inflate the mass of low-mass systems.

While the observed mass-to-light ratios are calculated

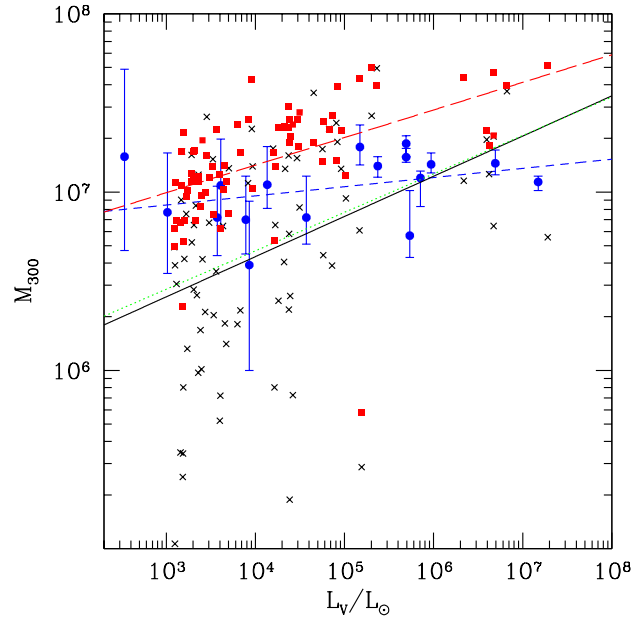


Figure 5. Scatter plot of M_{300} , the mass within 300 pc of the satellite center, versus satellite visual luminosity, L_V . Known MW satellites are represented by blue circles, while black x's denote il-luminated subhalos from our $(z_{\text{rei}}, z_{\text{H}_2}) = (11.2, 23.1)$ model with M_{300} measured directly from the simulation. Red squares show values of M_{300} measured, for each subhalo, at the time when the evolution in its maximum circular velocity has reached its peak and assuming an NFW profile. The short-dashed blue, solid black, dotted green, and long-dashed lines represent power-law fits of the $M_{300} - L_V$ relation respectively from observations, directly from the simulation, assuming NFW profiles for simulated subhalos today, and assuming NFW profiles for the subhalos when their maximum circular velocities peak.

from the mass within the stellar “tidal” radius, theoretical values from the simulation are computed using the mass within the dark matter tidal radius of the subhalo. This means that the model predictions are upper limits on the observed values. This is the best we can do without modeling the radial distribution of the stars within subhalos. The two definitions of mass-to-light ratio agree only in systems where the stars and the dark matter are truncated by tides at the same radius. Despite this difference, the model roughly reproduces the slope and amplitude of the relation between satellite mass-to-light ratio and visual luminosity. We do appear to produce extra faint halos with ratios even larger than observed, which most likely is a result of the definitional difference between the observed and theoretical values.

These results show that our model not only produces the correct abundance of luminous subhalos at each luminosity, but it also gives subhalos with approximately the correct physical properties for their luminosity. That is, the simulated subhalos that correspond to the brightest satellites or to the ultra-faint satellites in terms of their abundance have the same physical properties as the brightest or faintest satellites, respectively. Our faint objects do not, for example, have the physical properties, such as M_{300} or mass-to-light ratio, of the brightest satellites. This consistency increases confidence in our model.

Unfortunately, the different sets of model parameters

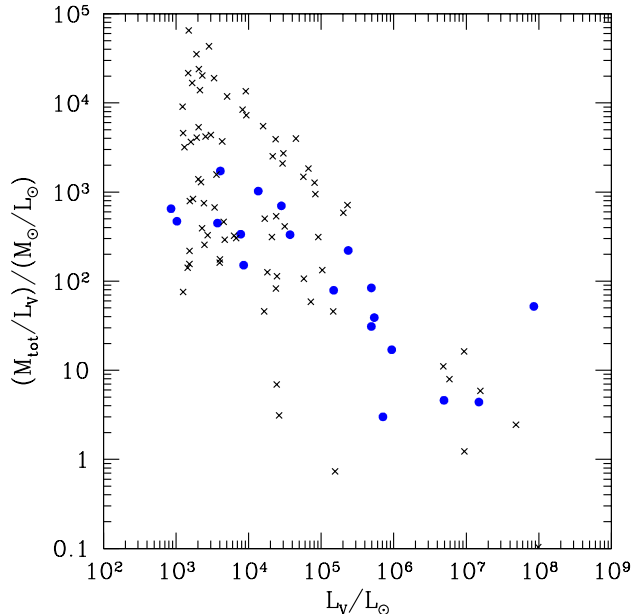


Figure 6. Scatter plot of the mass-to-light ratio of MW satellites versus their visual luminosities. Known MW satellites, whose ratios are calculated based on the mass within stellar “tidal” radii, are represented by blue circles. Black x’s denote illuminated subhalos from our $(z_{\text{rei}}, z_{\text{H}_2}) = (11.2, 23.1)$ model whose mass-to-light ratios were calculated using the simulated mass within their dark matter tidal radii.

we have been considering produce the about same range of M_{300} or mass-to-light ratio for a given luminosity. Of course, certain luminosities are under- or over-populated by points in different models, but these differences are better represented as differences in the luminosity function as we have described in §3.2. Therefore, these scatter plots are less useful for learning about reionization and star formation in the early universe.

4 DISCUSSION AND CONCLUSIONS

In this *Paper* we have shown that a physical model for star formation applied to the subhalos of a high-resolution galactic N-body simulation can, indeed, explain the full observed population of Milky Way (MW) dwarf satellites. While Macciò et al. (2009a) reached similar conclusions, they were not able to reproduce the faint end of the luminosity function (LF) because their model did not include molecular hydrogen cooling in halos with masses below $10^8 M_\odot$. Our inside-out model of the reionization of the MW galaxy forming region (MWgfr) is characterized by the star formation efficiency f_{H_2} , cooling mass M_{H_2} , and suppression redshift z_{H_2} of H_2 cooling, the normalized efficiency of H I -cooled stars $f'_{\text{H I}}$, normalized IGM clumping N'_{clump} , and the mean redshift of reionization \bar{z}_{rei} , and the star formation efficiency f_5 of massive systems capable of H I cooling after reionization. Here $N'_{\text{clump}} \equiv N_{\text{clump}} g(\delta) (1 - f_{\text{esc}})$ and $f'_{\text{H I}} \equiv f_{\text{H I}} g(\delta) / (1 - f_{\text{esc}})$. Our results are slightly at odds with recent measurements from the literature of M_{300} for ultra-faint systems, but we anticipate that measurement uncertainties may have resulted in the difference (see §3.3).

In §3.2, we used our model to explore what the observed LF of MW satellites could tell us about the early universe and discovered that satellites of different luminosities give clues about star formation at different epochs:

1. MW satellites with luminosities fainter than $M_V \approx -5$ can be explained by the inclusion of second-generation stars in low-mass halos above a cooling threshold of $M_{\text{H}_2} \sim 10^{5-6} M_\odot$ that were initially able to cool via molecular hydrogen in the very early universe.

We took advantage of the VLII’s high resolution to probe this process in very small systems and allowed for the possibility that a mechanism other than reionization was responsible for its suppression in the early universe. We have shown that our theoretical subhalos illuminated in this way are very faint, metal-poor (due to their very early creation), and have extreme mass-to-light ratios and the correct abundance to be responsible for the faintest population of satellites discovered in the SDSS DR5.

Using observations of these ultra-faint satellites to learn about the star formation process, we have found that molecular hydrogen cooling systems convert a fraction f_{H_2} of their initial gas into stars before star formation is suppressed very early in cosmic history at z_{H_2} . While the observed LF could not distinguish between models with $z_{\text{H}_2} = 23.1$ and $z_{\text{H}_2} = 17.9$, the radial distribution of these objects somewhat favors earlier suppression. The best fit values of the cooling mass and star formation efficiency for each value of z_{H_2} , assuming cosmic reionization at $\bar{z}_{\text{rei}} = 11.2$, are $(z_{\text{H}_2}, M_{\text{H}_2}/M_\odot, f_{\text{H}_2}) = \{(23.1, 10^5, 0.4), (17.9, 10^6, 0.04)\}$. Only if $\bar{z}_{\text{rei}} \lesssim 8$ is no H_2 cooling in low-mass systems required to reproduce the observed MW satellite LF. Confidence in our models increases when we note that our values of the cooling threshold are consistent with what has been already been assumed in simulations of the formation of the first stars (Whalen et al. 2008). Our results put further constraints on input parameters for these studies.

The physical difference between the two sets of $(z_{\text{H}_2}, M_{\text{H}_2}/M_\odot, f_{\text{H}_2})$ values that we considered may not be stark. The fact that f_5 increases for an earlier z_{H_2} may suggest a similarity with the inside-out reionization model of §2.2 where progenitors that reionized before the rest of the MWgfr have a star formation efficiency much greater than in an external reionization scenario. The similarities are intriguing, but we leave this problem to future work.

For either value of z_{H_2} that we considered, ultra-faint satellites are clearly the sites of the very first and oldest in the universe, and we agree that searches for these stars should be targeted there (Kirby et al. 2008; Frebel et al. 2009). While we do not expect stellar ages from future surveys precise enough to distinguish between formation at $z = 20$ and $z = 8$, the absence of any metal-poor stars older than 13 Gyr would represent a problem for our model.

Another interesting prediction for the future is the cutoff that we find in the luminosity of MW satellites. We have shown that the molecular hydrogen cooling mass and the associated star formation efficiency sets a minimum luminosity for satellites that cannot be significantly dimmer than what has already been observed. Interestingly, since the limit depends on the product $f_{\text{H}_2} M_{\text{H}_2}$, we find the same cutoff for both values of z_{H_2} considered. While our theoretical value is a bit brighter than that observed to date, the difference is

within the uncertainties in our calculation. A precise measurement of this minimum luminosity in the future would be a useful test of our model, which would not be able to explain satellites much dimmer than Segue 1.

2. The luminosity of satellites between $-5 > M_V > -9$ is dominated by stars produced through H I cooling of gas before the photoheating of the IGM at reionization.

We considered, for the first time, a model of reionization in the MWgfr with an inside-out morphology where dense progenitors more massive than the cooling mass, M_4 , reionize before the rest of the region. This prescription is based in the potentially large optical depth of Lyman-limit systems between the MW and the Virgo Cluster. We showed that this model explains the low star formation efficiency found in previous studies that assumed instantaneous, external reionization of the MWgfr, but both morphologies result in the same simulated observables.

We used the observed LF of satellites to probe \bar{z}_{rei} , the mean reionization redshift of all regions within the MWgfr. Depending on the choice of morphology, this represents either the redshift at which the MWgfr is quickly ionized by the Virgo Cluster or, since the overdensity of the IGM is small, the mean reionization redshift of the Universe. However, if the MWgfr does self-ionize, then we can learn not only about the efficiency of star formation but also about the clumpiness of the IGM.

After analyzing three possible values of \bar{z}_{rei} from VLII using the inside-out reionization prescription of §2.2, we found corresponding sets of model parameters that best fit the LF data: $(\bar{z}_{\text{rei}}, N'_{\text{clump}}, f'_{\text{H I}}, f_{\text{H 2}}) = \{(7.77, 7, 0.05, < 0.001), (9.14, 17, 0.2, 0.1), (11.2, 30, 1, 0.4)\}$; the values of $f_{\text{H I, ex}}$ for an external reionization scenario can be calculated from equation 4.

We find that the data is most consistent with early reionization at $\bar{z}_{\text{rei}} = 11.2$, consistent with the WMAP5 central value, and very high values for the clumpiness of the IGM, star formation efficiency, and escape fraction. This also implies a higher star formation efficiency in molecular hydrogen cooling systems at redshifts above $z \sim 20$ than for later reionization models. Our result also argues for early enrichment of the IGM (Furlanetto & Loeb 2003). Assuming consistency with WMAP results, simulations by Wise & Cen (2009) have found that, for a “normal” (i.e. non-topheavy) IMF, the product $f_{\text{H I}} f_{\text{esc}}$, averaged over atomic cooling halos with virial temperatures above 8000 K, to be 0.02 with $f_{\text{esc}} \sim 0.4$. This implies $g(\delta) \sim 12$ and that the cosmic IGM is relatively smooth with only a couple recombinations per baryon and a couple photons required, on average, to ionize each atom of hydrogen.

However, it remains possible that the discrepancy between the data and model predictions with later reionization results from a series of Poisson fluctuations or cosmic variance between VLII and the true MW history. In such a case, we are left with three possible points in parameter space. These points trace out a continuous path in the space of reionization parameters, but we were only able to probe discrete redshifts at which VLII slices have been analyzed. However, any external information about one of these parameters fixes a single point that fits the data reasonably well. For example, evidence that stars formed in molecular hydrogen cooling halos do not contribute to the luminosities of satellites today would argue for reionization around $\bar{z}_{\text{rei}} \approx 8$.

Finally, we note that the entire MWgfr need not reionize in one particular way; the dense progenitors could begin to self-ionize with radiation from the Virgo Cluster completing reionization for the rest of the region at some later time. The results we obtained by assuming an inside-out morphology for the entire MWgfr are valid as long as the progenitors of the MW satellites completely reionize themselves. This is because the satellite data is only sensitive to what happens in these objects. In this case, \bar{z}_{rei} is the mean reionization redshift of the Universe, since it is the time from which the stellar mass produced by MW progenitors to reionize themselves early is calibrated.

3. While stars formed before reionization do contribute somewhat to the luminosity of the brightest MW satellites ($M_V < -5$), this population of pre-SDSS objects can be explained by a combination of H I and metal-line cooling in the most massive subhalos after reionization.

These satellites were represented in our model by VLII objects that have exceeded a maximum circular velocity of V_5 sometime in their histories. When we included the pre-reionization stars and Orban et al. (2008) results to determine the stellar mass formed in the last 10 Gyr, we determined that a fraction $f_5 = 0.01$ of the photoheated gas retained by the largest subhalos after reionization is converted into stars. The majority of the gas must be kept hot or at low density to prevent these objects from being brighter than observed.

While old stars may be found in these satellites, they are not prime candidates for finding the relics of the first stars.

Although we have produced some interesting results using MW satellite data to probe the early universe, the data will become sensitive to the parameters of even more complicated models if: (1) additional new satellites are discovered to improve the statistics of the sample; (2) the errors on the M_{300} and the mass-to-light ratio of satellites are improved; (3) the degree of cosmic variance between different high-resolution MW simulations is understood; and (4) new high-resolution simulations are developed to include baryons and feedback processes. Progress is already being made on some of these fronts. PanSTARRS (Kaiser 2002), the Dark Energy Survey (Dark Energy Survey Collaboration 2005), SkyMapper (Keller 2007), and the Large Synoptic Survey Telescope (Ivezic et al. 2008) will intensively probe for satellites populating the galactic neighborhood. Additionally, Ishiyama et al. (2009) have compared subhalo populations for many different simulations of galactic halos and found more scatter than anticipated by Springel et al. (2008) using a smaller sample, but their work has not yet resolved the progenitors that formed ultra-faint systems. Once developed, high-resolution cosmological simulations with baryons and feedback will test much more specific models of reionization and open an avenue for comparisons with new observables, in addition to those explored here, such as the half-light radius, which promises to hold interesting clues about the high-redshift formation physics of MW satellites. With these improvements, our basic methodology can be used in the future to further probe reionization and the process of star formation in the early universe.

5 ACKNOWLEDGEMENTS

We thank Mike Kuhlen, Louie Strigari, Raja Guhathakurta, and Gerry Gilmore for useful discussions. J.D. acknowledges support from NASA through Hubble Fellowship grant HST-HF-01194.01. This research was supported in part by NASA grants NNX08AL43G and LA (A.L.), HST-AR-11268.01-A1 and NNX08AV68G (P.M.), and by Harvard University funds.

REFERENCES

- Abel, T., Bryan, G. L., & Norman, M. L. 2002, *Science*, 295, 93
- Alvarez, M. A., Busha, M. T., Abel, T., & Wechsler, R. H. 2009, arXiv:astro-ph/0812.3405
- Barkana, R., & Loeb, A. 2001, *Physics Reports*, 349, 125
- . 2004, *ApJ*, 609, 474
- Belokurov, V. 2009, arXiv:astro-ph/0903.0818
- Benson, A. J., Frenk, C. S., Lacey, C. G., Baugh, C. M., & Cole, S. 2002, *MNRAS*, 333, 177
- Bovill, M. S., & Ricotti, M. 2008, arXiv:astro-ph/0806.2340
- Bromm, V., Kudritzki, R. P., & Loeb, A. 2001, *ApJ*, 552, 464
- Bromm, V., & Larson, R. B. 2004, *ARAA*, 42, 79
- Bromm, V., & Loeb, A. 2003, *Nat*, 425, 812
- Bruzual, G., & Charlot, S. 2003, *MNRAS*, 344, 1000
- Bullock, J. S., Kravtsov, A. V., & Weinberg, D. H. 2000, *ApJ*, 539, 517
- Busha, M. T., Alvarez, M. A., Wechsler, R. H., Abel, T., & Strigari, L. E. 2009, arXiv:astro-ph/0901.3553
- Dark Energy Survey Collaboration. 2005, arXiv:astro-ph/0510346
- Diemand, J., Kuhlen, M., & Madau, P. 2007, *ApJ*, 667, 859
- Diemand, J., Kuhlen, M., Madau, P., Zemp, M., Moore, B., Potter, D., & Stadel, J. 2008, *Nat*, 454, 735
- Faucher-Giguère, C.-A., Lidz, A., Hernquist, L., & Zaldarriaga, M. 2008, *ApJ*, 688, 85
- Frebel, A., Simon, J. D., Geha, M., & Willman, B. 2009, arXiv:astro-ph/0902.2395
- Furlanetto, S. R., & Loeb, A. 2003, *ApJ*, 588, 18
- Gilmore, G., Wilkinson, M. I., Wyse, R. F. G., Kleyna, J. T., Koch, A., Evans, N. W., & Grebel, E. K. 2007, *ApJ*, 663, 948
- Gnedin, N. Y. 2000, *ApJ*, 542, 535
- Gnedin, N. Y., & Kravtsov, A. V. 2006, *ApJ*, 645, 1054
- Haiman, Z., Abel, T., & Rees, M. J. 2000, *ApJ*, 534, 11
- Haiman, Z., Rees, M. J., & Loeb, A. 1997, *ApJ*, 476, 458
- Ishiyama, T., Fukushige, T., & Makino, J. 2009, *ApJ*, 696, 2115
- Ivezic, Z., Tyson, J. A., Allsman, R., Andrew, J., Angel, R., & for the LSST Collaboration. 2008, arXiv:astro-ph/0805.2366
- Kaiser, N. 2002, in *Proceedings of the SPIE*, Vol. 4836, Society of Photo-Optical Instrumentation Engineers (SPIE) Conference Series, ed. J. A. Tyson & S. Wolff, 154–164
- Keller, S. C. 2007, *Publ. Astron. Soc. Australia*, 24, 1
- Kirby, E. N., Simon, J. D., Geha, M., Guhathakurta, P., & Frebel, A. 2008, *ApJ*, 685, L43
- Komatsu, E. 2009, *ApJS*, 180, 330
- Koposov, S., Belokurov, V., Evans, N. W., Hewett, P. C., Irwin, M. J., Gilmore, G., Zucker, D. B., Rix, H.-W., Fellhauer, M., Bell, E. F., & Glushkova, E. V. 2008, *ApJ*, 686, 279
- Koposov, S. E., Yoo, J., Rix, H.-W., Weinberg, D. H., Macciò, A. V., & Miralda-Escudé, J. 2009, ArXiv e-prints
- Kravtsov, A. V., Gnedin, O. Y., & Klypin, A. A. 2004, *ApJ*, 609, 482
- Li, Y.-S., Helmi, A., De Lucia, G., & Stoehr, F. 2008, arXiv:astro-ph/0810.1297
- Macciò, A. V., Kang, X., & Moore, B. 2009a, *ApJ*, 692, L109
- Macciò, A. V., Kang, X., Fontanot, F., Somerville, R. S., Koposov, S. E., & Monaco, P. 2009b, arXiv:astro-ph/0903.4681
- Madau, P., Diemand, J., & Kuhlen, M. 2008a, *ApJ*, 679, 1260
- Madau, P., Kuhlen, M., Diemand, J., Moore, B., Zemp, M., Potter, D., & Stadel, J. 2008b, *ApJ*, 689, L41
- Martin, N. F., Ibata, R. A., Chapman, S. C., Irwin, M., & Lewis, G. F. 2007, *MNRAS*, 380, 281
- Mateo, M. L. 1998, *ARAA*, 36, 435
- Moore, B., Diemand, J., Madau, P., Zemp, M., & Stadel, J. 2006, *MNRAS*, 368, 563
- Moore, B., Ghigna, S., Governato, F., Lake, G., Quinn, T., Stadel, J., & Tozzi, P. 1999, *ApJ*, 524, L19
- Navarro, J. F., Frenk, C. S., & White, S. D. M. 1997, *ApJ*, 490, 493
- Orban, C., Gnedin, O. Y., Weisz, D. R., Skillman, E. D., Dolphin, A. E., & Holtzman, J. A. 2008, *ApJ*, 686, 1030
- Ricotti, M., & Gnedin, N. Y. 2005, *ApJ*, 629, 259
- Ricotti, M., Gnedin, N. Y., & Shull, J. M. 2002a, *ApJ*, 575, 33
- . 2002b, *ApJ*, 575, 49
- Salvadori, S., & Ferrara, A. 2008, ArXiv e-prints
- Sheth, R. K., & Tormen, G. 1999, *MNRAS*, 308, 119
- Simon, J. D., & Geha, M. 2007, *ApJ*, 670, 313
- Somerville, R. S. 2002, *ApJ*, 572, L23
- Spergel, D. N., Bean, R., & Doré, O. 2007, *ApJS*, 170, 377
- Springel, V., Wang, J., Vogelsberger, M., Ludlow, A., Jenkins, A., Helmi, A., Navarro, J. F., Frenk, C. S., & White, S. D. M. 2008, *MNRAS*, 391, 1685
- Strigari, L. E., Bullock, J. S., Kaplinghat, M., Diemand, J., Kuhlen, M., & Madau, P. 2007, *ApJ*, 669, 676
- Strigari, L. E., Bullock, J. S., Kaplinghat, M., Simon, J. D., Geha, M., Willman, B., & Walker, M. G. 2008, *Nat*, 454, 1096
- Tollerud, E. J., Bullock, J. S., Strigari, L. E., & Willman, B. 2008, *ApJ*, 688, 277
- Whalen, D., van Veelen, B., O’Shea, B. W., & Norman, M. L. 2008, *ApJ*, 682, 49
- Wise, J. H., & Cen, R. 2009, *ApJ*, 693, 984